Russian Physics Journal, Vol. 51, No. 10, 2008

GAMMA-RAY DETECTORS BASED ON GaAs<Cr> FOR NANOSTRUCTURAL INVESTIGATIONS

G. I. Ayzenshtat,[1] D. L. Budnitskii,[2] D. Yu. Mokeev,[1] V. A. Novikov,[1] E. M. Syresin,[3] O. P. Tolbanov,[2] A. V. Tyazhev,[2] G. A. Shelkov[3]

UDC 621.382.2

The progress in nanotechnologies has been largely due to the advent of a new generation of gamma-ray sources and position detectors, which can ensure both coordinate and temporal measurements within the nano- and femtoranges. The paper offers scientific and engineering solutions related to designing detector materials and structures for detecting single quanta of x- and γ-rays and high-energy charged particles. These are multi-element position detectors of a new generation for nanostructure imaging and examination in gamma rays.

INTRODUCTION

The development of the fundamental science and in particular its practical applications cannot be thought of without devices for viewing and measuring of nanostructures. The use of the visible light in a wide class of optical devices such as microscopes has made it possible to view, measure, and design objects of micron sizes. Further size reduction is impossible due to a principal limitation of the finite visible light wavelength ($\lambda \sim 1$ μm). The electromagnetic waves of shorter wavelengths are ultraviolet radiation and x-rays (γ-rays).

ADVANCED X-RAY SOURCES

The growth of the technological and applied research sectors demanded that advanced x-ray sources of coherent radiation within a wide wavelength range be designed, which could ensure better performance than conventionally available x-ray tubes. These are synchrotron radiation sources that have become today a necessary attribute for the hi-tech development.

SYNCHROTRON SOURCES

Synchrotron radiation results from the motion of a charged particle in the magnetic field. The intensity of synchrotron radiation is inversely proportional to the particle mass squared, therefore, synchrotron radiation sources are designed on the basis of electron synchrotrons. The maximum of synchrotron radiation spectrum is at the wavelength $\lambda_c \approx R / \gamma^3$ depending on the relativistic factor γ and radius R of the electron trajectory in synchrotron rotation magnets. The synchrotron radiation with the wavelength ~1 nm can be effectively used in nanotechnology. To generate the radiation with the indicated wavelength in the electron synchrotrons with $R \sim 10$ m, electrons should have the energy ~1 GeV. Synchrotron radiation is widely used in physical, biological, medical, chemical, and geological research and contributes to the development of nanotechnologies, in particular, micromechanics and microelectronics. Thus, in

[1]Tomsk State University, Tomsk, Russia, [2]V. D. Kuznetsov Siberian Physical-Technical Institute of Tomsk State University, Tomsk, Russia, e-mail: tolbanov@rid.tom.ru; [3]Joint Institute for Nuclear Recearch, Dubna, Russia. Translated from Izvestiya Vysshikh Uchebnykh Zavedenii, Fizika, No. 10, pp. 38–52, October, 2008. Original article submitted June 10, 2008.

1064-8887/08/5110-1037 ©2008 Springer Science+Business Media, Inc.

lithography, the deposition of conducting layers of a given configuration on the crystal surface makes it possible to make elaborate microelectronic circuits. The integrated microcircuits with the size 2–3 μm require the use of UV lasers. The synchrotron radiation at ~1 nm enables one to design microcircuits in the nanometer range using nanotechnological processes. One of the key characteristics of the radiation is its brightness – the number of γ-photons per unit time, unit spatial angle, unit area, and 0.1% of the radiation bandwidth. The brightness of conventionally available synchrotron sources is 10^{24}–10^{25} photon/(s·mrad^2·mm^2·0.1% b.w.). A further increase in the brightness of synchrotron radiation is limited by its nonmonochromaticity $\Delta\lambda/\lambda \sim 1$, angular divergence $\theta \sim \gamma^{-1}$, and the duration (~1 ns) and incoherence of a detected radiation pulse. Over the years of extensive use of synchrotron sources, a demand arouse for developing a new generation of gamma-ray sources, that is, the sources of femtosecond pulses of coherent gamma radiation based on X-Ray Free Electron Lasers (XFEL).

SOURCES OF FEMTOSECOND PULSES OF COHERENT GAMMA RADIATION ON THE BASIS OF X-RAY FREE ELECTRON LASERS (XFEL)

For generation of monochromatic radiation of high brightness and with tunable wavelength, use is made of X-Ray Free Electron Lasers (XFEL). In these lasers, a relativistic electron beam transmitted through an undulator is a working medium. The undulator is a device where a vertical magnetic field varying along the direction of electron-beam propagation according to the harmonic periodic law is generated. In the course of beam transmission through the first undulator periods, the electron beam density is modulated at the radiation wavelength due to initial noises of the electron beam and synchrotron radiation. The phase modulation of the electron-beam density results in further increase in the radiation intensity and density modulation depth.

As a result, the radiation intensity is exponentially increased with the undulator length by 6–7 orders of magnitude as compared to its initial level. The radiation intensity is saturated at a certain undulator length, where all beam electrons emit in one phase due to deep modulation of the beam density. The maximum brightness of X-Ray Free Electron Laser radiation is 6–7 orders of magnitude higher than that of conventional sources of synchrotron radiation. In this laser, the radiation wavelength can be easily varied with the electron energy. The wavelength is proportional to the undulator period length d and inversely proportional to the relativistic factor squared $\lambda \propto d/\gamma^2$. At the electron energy 10 GeV and undulator period $d \sim 4$ cm, the wavelength is $\lambda \sim 0.1$ nm. In this case, the wavelength is lower than or comparable to the atomic size. The variation of the radiation wavelength is one of the key advantages of the X-Ray Free Electron Laser in comparison with the conventional ones.

The X-Ray Free Electron Laser possesses a number of additional advantages. The electron beams with the average power of some tens of megawatts and average power density up to 100 MW/mm^2 make it possible to produce X-Ray Free Electron Lasers with the average radiation power ~10 MW. The use of an electron beam as a working medium ensures low angular (diffraction) divergence of radiation. The undulator radiation in the X-Ray Free Electron Laser is coherent. The monochromaticity of radiation is about $\Delta\lambda/\lambda \sim 10^{-3}$. The pulse duration of coherent radiation is in the femtosecond range $\tau \sim (\lambda/c)\cdot(\lambda/\Delta\lambda) \sim 1$ fs, which corresponds to the characteristic atomic times of electron transition from one level to another. In this case, the use of the X-Ray Free Electron Laser makes it possible to go from the time-averaged photography to filming in the femtosecond time scale.

The use of monochromatic radiation with subnanometer wavelength and femtosecond resolution offers new possibilities in investigating chemical and physical processes in atoms and designing new materials and structures. This, first and foremost, is concerned with the development of new semiconductors as well as magnetic, optical, and biological sensors. One of the most important directions in nanotechnology is new magnetic carriers whose size is smaller than 100 nm. The development of structures of quantum electronics on the basis of semiconductor materials calls for investigations at the atomic level. Thus, for example, investigations of an individual island or several connected islands in InGaAs/GaAs structures with quantum dots allow one to produce semiconductors with certain specified properties. Using x-ray laser radiation one can measure transitions to neutral and charged single excitons in the quantum-dot structures.

Coherent radiation with femtosecond resolution and nanometer wavelength can well be used for investigations into the dynamics of a crystal surface and dynamic processes in metals, alloys, and ceramics. The use of high-power

x-ray radiation of nanometer wavelength is of great importance for realizing nanotechnologies in micromechanics and for development of such engineering processes as laser cutting, drilling, and processing.

At the Joint Institute for Nuclear Research (JINR), the work on X-Ray Free Electron Laser is performed in three directions. An X-Ray Free Electron Laser designed for radiation generation in the IR and UV ranges is being developed on the basis of a linear JINR accelerator – Linak-800 [1]. Within the framework of cooperation with the Deutche Electronen Synchrotron, Germany (DESY), the JINR is working out accelerators and test equipment for a Free Electron Laser FLASH [2, 3] generating radiation with the wavelength higher than 6 nm. Within the Russian Program on Nanotechnologies, the work on development of the European X-Ray Free Electron Laser has already started [4].

ADVANCED GAMMA-RAY DETECTORS

The discovery of the above-mentioned sources of electromagnetic waves with shorter wavelengths (X-ray radiation with energies up to ~15 keV or $\lambda \sim 0.1$ nm – characteristic atomic size) has made it possible to design microscopes of a new generation capable of efficient detecting of images in the x-ray with the energy of 1–15 keV. The discovery of the electromagnetic field demanded that the devices for emission, reception, amplification, and reproduction of electromagnetic waves in a wide spectral range be designed. Thus, the epoch of radiophysics has evolved that gave rise to a variety of scientific directions, including semiconductor materials science and microelectronics. The development of radiophysics resulted in modern radar and telecommunication systems.

However, a radio frequency band takes only about a quarter of the total electromagnetic scale extending up to 30 orders of quantum energies. Radiation in the range of quantum energies higher than the energy of electron-hole pair formation in semiconductors (3–4 eV) covers about 14 orders of magnitude of energy and is referred to as ionizing radiation. A special feature of ionizing radiation is its high penetrability proportional to energy. For example, all objects are transparent in the x- and gamma-rays. The radiation transmitted through an object carries information on the intrinsic properties of the object because the radiation intensity and energy spectrum are changed. These characteristics can be used to construct images of object anatomy.

In the ultra-violet region of spectrum, the problem is to develop technical means for detecting ionizing radiation. Since the discovery of ionizing rays (α, β, γ, χ) there has been the problem of designing tools for detecting single quanta and determining their energy and coordinates. By analogy with radiophysics, these devices were referred to as detectors. The urgency and scale of research in this direction are beyond question. The main impediment to the development of experimental nuclear physics has always been the design of ionizing radiation detectors. The importance of designing of these new types of detectors is supported by the fact that more than ten new types of detectors were designed only in the past century. Three of these (the Wilson chamber, the bubble chamber, and the ionization chamber) have made their authors the Nobel Prize winners [5].

Since the seventies of the last century, semiconductor materials have been widely used in detectors. Modern high-energy experimental physics cannot do without semiconductor detectors. The scale of application of semiconductor detectors in high-energy physics can be illustrated by an example of the international project ATLAS at LHC (CERN, Switzerland) with the budget higher than 500 million US dollars. The pixel detectors within the framework of this project have the total area 2 m^2 and contain 140 million of sensor elements (pixels). The microstripped detectors have the total area of 60 m^2 and contain more than 6 million stripped elements [6]. The extended use of solid detectors gave rise to the corresponding research direction in semiconductor physics. The direction evolved in three steps. In the early seventies, the first semiconductor detectors based on the lithium compensated Si and Ge were designed. In the late eighties, spectrometric detectors based on pure Si and Ge were developed. A new step in production of detectors based on complex semiconductor compounds started less than 10 years ago. Currently, the most popular binary and ternary compounds are the GaAs, CdTe, and CdZnTe semiconductors. The latter two should rather be considered as future candidate materials due to their high price and lack of technology for production [7].

Increased interest to semiconductor detectors has, for more than 30 years, been due to their high-energy resolution. In addition, the semiconductor detectors possess the highest speed of response and coordinate resolution as compared to their vacuum and scintillation analogs. This made it possible to extend the application area of the detectors

based on compound semiconductors, in particular, those on the basis of GaAs. Multi-element detectors hold the most promise for designing of the following devices:

- Low-dose digital medical tomographs, mammographs, dental apparatus, systems for monitoring of cancer tumors and x-ray diagnosis of bone diseases;
- Defectoscopes and laminographs with high spatial resolution up to 0.02 mm;
- High-efficiency systems for customs inspection and monitoring systems for handling of hazardous commodities;
- Low-dose safety systems at airports, railway stations, and thoroughfares designed to reduce the probability of terrorist attacks in public places.

Research into detectors being performed in Tomsk is aimed at solution of the foregoing problems and includes the following directions:

- Simulation and experimental examination of transport and collection of non-equilibrium charge carriers from ionization α, β, and γ tracks in microstripped and pixel detector structures;
- Technology of detector materials and structures (GaAs and related compounds) including compensation by deep-level impurities during diffusion and gas-phase and liquid-phase epitaxy;
- Exploration of electrophysical, photoelectrical and pulse characteristics of the detector materials, structures, and detectors;
- Design of different constructions and technologies for quantum-sensitive detectors of α, β, γ, and χ, neutron, and ion radiation;
- Design and production of microstripped and pixel position detectors and new-generation detectors of x-ray and gamma-ray images;
- Design, fabrication, and assembly of digital image modules for multi-purpose digital information and monitoring systems;
- Development of digital x-ray facilities for medical and technical purposes on the basis of quantum-sensitive detectors and digital image modules.

In this work, the main directions of research into detectors performed by Tomsk scientists are summarized. The results of these investigations are reported in [8–45].

BASIC PHYSICS OF OPERATION OF QUANTUM-SENSITIVE DETECTORS

Semiconductor detectors are solid ionization chambers, where the drift region of nonequilibrium charge carriers is a sensitive element. Particle and photon energy recorded by the detector is such that most of the particle energy loss is spent to generate electron-hole pairs. The total number of nonequilibrium charge carriers in the track is $N_0 = E_0/E_i$, where E_0 is the energy lost by a particle in the semiconductor volume and E_i is the energy spent by a particle on ionization of one electron-hole pair. A significant advantage of semiconductor detectors is a low value of E_i, which is about 3–4 eV for most semiconductors. If the potential difference (U) is applied to the detector, the nonequilibrium charge carriers drift from the track to the corresponding electrodes and induce a pulse of current in the external circuit. In accordance with the Ramo–Shockley theorem, the current induced by drift of a single charge (e) is determined by the scalar product of the electric field vector (ξ) and drift velocity vector (υ): $i_{\text{ind}} = e \cdot \xi_\upsilon \cdot \upsilon$, where $\xi_U = \xi / U$. If the drift space represents a d-thick plane capacitor, where the charge moves with the velocity vector parallel to the electric field vector, the induced current can be described as $i = e \cdot \upsilon / d$, where υ is the projection of the velocity vector onto the field vector. In fact, a packet of electron-hole pairs with the concentration N_o is formed in the ionization space upon absorption of a single particle. The current induced on electrodes is a sum of elementary currents [46], and we have

$$i_n = e \cdot \upsilon_n \cdot N_0 / d, \quad i_p = e \cdot \upsilon_p \cdot N_0 / d, \tag{1}$$

where

$$\upsilon_n = \mu_n \cdot \xi, \quad \upsilon_p = \mu_p \cdot \xi \tag{2}$$

are the averaged drift velocities determined by electron μ_n and hole μ_p mobilities, provided that the electric field is uniformly distributed, that is, $\xi(x) = \text{const}$. When the electron and hole packets move in the interelectrode space, a part of charge carriers either recombines or is at the attachment centers and therefore does not reach the electrodes. Therefore, the real free paths of charge carriers contributing to the induced current are determined by the electron and hole drift lengths L_n and L_p in the time τ_n and τ_p as

$$L_n = \upsilon_n \cdot \tau_n \quad L_p = \upsilon_p \cdot \tau_p \,. \tag{3}$$

Let us introduce the quantity $\eta(x)$ determining the part of charge carriers, which reached the contacts. In this case, the relation, $\eta(x) = \bar{N} / N_0 = (e \cdot N)/(e \cdot N_0) = \bar{Q} / Q_0$ is valid, where $\bar{N}$ is the mean concentration of charge carriers at the contacts, Q_0 is the charge of free carriers in a single- particle track, Q is the mean charge of the carriers at the contacts. The quantity $\eta(x)$ is referred to as the charge collection efficiency (CCE) and is one of the most important characteristics of detector operation. For a plane capacitor, the probability of collection of electron-hole pairs formed at an arbitrary distance x from the cathode is [47]

$$\text{CCE} = \frac{\bar{Q}}{Q_0} = \frac{1}{d}\left[L_n \left(1 - \exp\left(-\frac{d-x}{L_n}\right)\right) + L_p \left(1 - \exp\left(-\frac{x}{L_p}\right)\right)\right]. \tag{4}$$

It follows from Eq. (4) that CCE is found from the drift lengths of nonequilibrium electrons and holes. We consider the γ-quantum absorption in the sensitive layer of detector. At high values of drift lengths of nonequilibrium electron-hole pairs in the track, for which the relation $L_n > d, \quad L_p > d$ is fulfilled, the exponents in the right-hand side of Eq. (4) can be expanded in series, and we have

$$\text{CCE} = \frac{L_n}{d}\left[1 - \left(1 - \frac{d-x}{L_n}\right)\right] + \frac{L_p}{d}\left[1 - \left(1 - \frac{x}{L_p}\right)\right] = \frac{d-x}{d} + \frac{x}{d} = 1 \,.$$

Thus, $\text{CCE} = 1$, independent of the coordinate of formation of the electron-hole pair packet. Then, the amplitude spectrum is a narrow monoenergy line corresponding to the condition $N_0 = E_0/E_i$. This is a key condition for operation of spectrometric detectors. In the case of asymmetry of electron and hole drift lengths, for instance, $L_p << L_n$, it follows from Eq. (4) that $\text{CCE} = \frac{d-x}{d} = 1 - \frac{x}{d}$. That is, CCE is a function of the coordinate of nonequilibrium charge-carrier packet formed by absorption of a single particle. At $x \to 0$ (absorption of a γ-quantum near the cathode), CCE → 1, and at $x \to d$ (absorption of a γ-quantum near the anode), CCE → 0. For the electron drift length $L_n < d$, we can neglect the exponent in Eq. (4). In this case, CCE ≈ L_n/d, that is, it is independent of the coordinate, where the γ-quantum is absorbed, and is limited by the electron drift length. In essence, the field dependence CCE(ξ) corresponds to that of the drift length $L_n(\xi)$ in the structures with thick high-resistance layers, where the condition $d > L_n$ is fulfilled. It is shown in [48] that the experimental amplitude spectra and field dependence of the charge collection efficiency is well described by Eq. (4), provided the relations $L_n(\xi)/d$ and $L_p(\xi)/d$ are known.

CHARACTERIZATION OF DETECTOR MATERIALS AND STRUCTURES

It is rightly assumed that purity of semiconductor materials determines the effective operating capacity of particle detectors and their basic characteristics. The residual background impurity concentration (N_b) specifies the form of the distribution of electric field strength $\xi(x)$ in the structure. Therefore, purity of materials eventually limits the

thickness of the sensitive layer in detectors. In the presence of a potential barrier and a constant concentration of background impurities, the penetration depth of the electric field into the structure is $d_0(\xi) = 3.5 \cdot 10^3 \sqrt{U / N_b}$ [cm]. Thus, for the lowest achievable background-impurity concentration in silicon $N_b \approx 4 \cdot 10^{12}$ cm^{-3} and bias voltage $U = 300$, we have $d_0 \approx 300$ μm. It is this depth that determines the detection efficiency described by the Bouguer law. On the other hand, the nonequilibrium charge-carrier drift length being the function of the electron and hole lifetimes and drift velocities determines the efficiency of charge collection in accordance with Eq. (3). In pure semiconductors, the electron and hole lifetimes have similar high values, and the relations $L_n(\xi) > d(\xi)$ and $L_p(\xi) > d(\xi)$ are fulfilled. Therefore, in accordance with Eq. (4), the efficiency of charge collection is $\eta \to 1$. Due to this, semiconductor detectors for spectrometric purposes are mainly constructed on the basis of pure elementary Si or Ge semiconductors. Undoubtedly, these semiconductors have advantages at low temperatures. However, at high temperatures, narrow energy-gap widths have an adverse effect. In addition, pure materials are not, in essence, radiation-resistant ones. For example, under absorption of the proton radiation dose $\geq 10^{12}$ cm^{-2}, the charge-carrier lifetime in Si decreases by a factor of 3–4, which results in the corresponding increase in dark current and detector degradation.

Higher energy-gap binary and ternary semiconductors such as GaAs will become an alternative in the nearest future. Inherently, compound semiconductors are more radiation-resistant. Their higher energy-gap width causes lower leakage currents. On the other hand, compound semiconductors, as a rule, exhibit asymmetry of the drift length, and the CCE is found from the biggest drift length of nonequilibrium charge carriers in the track (Eq. (4)).

INGOT SEMIINSULATING GaAs (SI-GaAs)

Liquid encapsulated Czochralski technique (LEC) is traditionally used in the world's practice for growing semiinsulating GaAs (SI-GaAs) compensated by the deep donor *EL*2-centers [49]. The donor *EL*2-centers in the $EL2^+$ state have a giant electron capture cross-section of about $\approx 1 \cdot 10^{-13}$ cm^2 [50, 51] limiting the electron lifetime to the values of $\tau_n^{max} = 1 / \sigma^-_{EL2^+} \cdot \upsilon_n \cdot N_{EL2^+} \approx 0.2$ ns, which decreases the electron drift length and causes low collection efficiency of the electron component of charge. This is supported by the results reported in [52, 53], where the shape of a detector current pulse was analyzed and a conclusion was made that the hole component of charge composes the major part of the current pulse induced in the external circuit. It is shown in [54–56] that with the increase in the specific resistance of the LEC SI-GaAs-structures, one can observe a proportional decrease of the CCE, nonequilibrium electron lifetime, and thickness of the detector active region. One of the key problems limiting wide use of LEC SI-GaAs for detectors is the nonuniform distribution of the electric field strength $\xi(x)$ in depth of the detector. In addition, at a relatively low mean value of field of $\langle\xi\rangle \approx 1$ kV/cm, current oscillations are generated in the external circuit [57]. There are a number of physical models showing that these experimentally observed oscillations are slow recombination domains. For visual observation of domain origin and motion patterns in a detector structure, use was made of a technique based on the Franz–Keldysh effect. This technique is based on the field dependence of absorption coefficient near the fundamental absorption edge of a semiconductor. IR-radiation is applied to the end of the sample under study, where the electric field distribution $\xi(x)$ is preset by applying a bias voltage to the external electrodes. The radiation transmission coefficient of the detector structure is varied in accordance with the $\xi(x)$ distribution. The transmitted radiation is transformed into an image on the monitor using a digital camera. We have measured tens of different structures. Analysis of the experimental data shows that a nonuniform distribution of $\xi(x)$ is observed for all SI-GaAs structures grown using the LEC technology independent of the manufacturer. By means of motion-picture recording, we also observed the dynamics of this process in the form of dark clusters, corresponding to the electric field oscillations, moving through the structure. The deepest penetration depth of the electric field into the sample is 200–250 μm, which limits the thickness of the sensitive layer in LEC SI-GaAs-structures.

Cr-COMPENSATED SI-GaAs

There are two ways of decreasing the $EL2^+$-center concentration [58]:

- To decrease the growth temperature of undoped SI-GaAs, which calls for application of epitaxial technology;
- To fill the centers by electrons in the equilibrium state: $EL2^{+} + e \rightarrow EL2^{0}$, which is possible, if a shallow donor impurity with the concentration $N_d > N_{EL2}$ and a compensating deep acceptor Cr impurity with the concentration $N_{\text{Cr}} > N_{EL2}$ are introduced into crystals during their growth.

The production and investigation of epitaxial materials of detector quality are discussed in detail in [58, etc.] and are not the subject of this paper.

We developed a technology for compensation of the n-type GaAs layers by diffusion of a deep acceptor Cr impurity [58, etc.]. The technology allows us to control the deep impurity dissolution and diffusion processes in a wider temperature range as compared with epitaxy. For this purpose, we use GaAs doped by tin with the electron concentration $n \cong N_d$. On introducing the Cr atoms with the concentration $N_{\text{Cr}} > N_d > N_f$, where N_f is the total concentration of intrinsic defects and background impurities, GaAs is recompensated into the *i*-type of conductivity. Diffusion of the deep Cr impurity occurs at high temperatures, therefore, the compensation processes are accompanied by reconstruction of the intrinsic defects. As a result, high compensation by deep centers is achieved, the Fermi level occupies the limit position F_{lim} in the bulk, and the specific resistance ρ attains its highest value [59]: $\rho_i \cong \rho_{\max} = 1/2e \cdot \sqrt{\mu_n \cdot \mu_p} \cdot n_i$, where n_i is the intrinsic concentration. The experimental specific resistance for these structures is $\geq 1 \cdot 10^{9}$ Ω·cm, which is more than one order of magnitude higher than that of LEC SI-GaAs-based structures. This causes the transition from the barrier-type structures to the resistive-type ones. For these structures, ohmic contacts are used, which favors the uniform distribution $\xi(x)$ over the whole thickness of the structure. Thus, $d(\xi) \equiv d_0$, where $d(\xi)$ is the sensitive layer thickness. The volt-ampere characteristics of resistive-type structures are linear and symmetric up to the electric field strengths corresponding to the maximum drift velocities. The current density in the structure does not exceed 10^{-8} A/mm^2 at the working bias voltage.

Complete collection of nonequilibrium charge carriers from the track corresponds to the condition $L_{d_n} = \tau_n \cdot \upsilon_n(\xi) > d(\xi)$, $L_{d_p} = \tau_p \cdot \upsilon_p(\xi) > d(\xi)$ in the sensitive layer. In the compensated structures, the charge-carrier drift length significantly increases, which is suggested by the experimental data. The most important difference between our and conventional LEC SI-GaAs structures is in the uniform distribution of $\xi(x)$ and the absence of current oscillations.

ELECTROPHYSICAL PARAMETERS OF DETECTOR STRUCTURES

There are a number of the most important parameters which determine the quality of detector structures and detectors.

Efficiency of radiation recording. If radiation with the initial intensity I_0 is incident onto the detector surface area S in unit time t, the number of absorbed quanta is

$$N_0 = \Delta I \cdot S \cdot t = I_0 \cdot S \cdot t \cdot [1 - \exp(-\alpha \cdot d_n)], \tag{5}$$

where α is the radiation absorption coefficient and d_n is the absorption layer thickness. If the absorption coefficient determined by the GaAs density and nuclear charge of Ga and As atoms is a basic characteristic of the material, an increase in the absorption layer thickness depending on the problem under study is specified by the detector construction.

Charge collection efficiency (CCE) under absorption of a single quantum determines the detector sensitivity to radiation. According to Eq. (4), the CCE is determined by the drift lengths (L_n, L_p) of the nonequilibrium charge carriers as follows:

$$L_n(\xi) = \tau_n \cdot \upsilon_n(\xi), \quad L_p(\xi) = \tau_p \cdot \upsilon_p(\xi), \quad \upsilon_n(\xi) = \mu_n \cdot \xi(x,t), \quad \upsilon_p(\xi) = \mu_p \cdot \xi(x,t). \tag{6}$$

These relations show that, eventually, the problem of finding the drift length can be reduced to finding two electrophysical parameters of the structure: the charge-carrier lifetimes τ_n and τ_p and the electric-field distribution $\xi(x)$. This is confirmed by the results of modeling of charge transport and collection and by the results of calculations provided that $\xi(x)$ gives the limiting drift velocity υ_s of nonequilibrium electrons and holes in the entire sensitive volume.

Charge-carrier drift length in high-resistance structures was determined experimentally from analysis of the field dependence of α-spectra. In the experiment, the condition $d_0 >> L_\alpha$ was fulfilled, where L_α is the α-particle Bragg absorption length (in GaAs, $L_\alpha \approx 20$ μ). Therefore, to a certain degree of approximation, α-particles can be assumed to be absorbed in the near-surface layer. Then, depending on the bias voltage polarity, either electron or hole drift occurs in the high-resistance layer. For example, assuming in Eq. (4) $x \to 0$ and taking into account Eq. (6), we obtain for the electron drift that

$$Q_\alpha(U) = Q_0 \frac{\mu_n \cdot \tau_n \cdot U_0}{d_0^2}\left[1 - \exp\left(-\frac{d_0^2}{\mu_n \cdot \tau_n \cdot U_0}\right)\right], \tag{7}$$

where $Q_0 = e(E_\alpha / E_i)$ is the charge formed in the structure by a single α-particle. Comparison shows that the experimental dependence $Q_\alpha(U)$ and Eq. (7) are in qualitative agreement. Since at the low bias voltage U_0, the bracketed expression tends to unity, the dependence $Q_\alpha(U)$ can be approximated by a straight line with the slope $\mu_n \cdot \tau_n \cdot Q_0 / d_0^2$. From the slope, we can experimentally determine the products $\mu_n \cdot \tau_n$, $\mu_p \cdot \tau_p$ at various bias voltages and construct the field dependences of drift lengths as follows:

$$L_n = \mu_n \cdot \tau_n \cdot U / d_0, \quad L_p = \mu_p \cdot \tau_p \cdot U / d_0 . \tag{8}$$

An analysis of experimental data shows that at the electric-field strength $\langle\xi_{av}\rangle \geq$ 30–40 kV/cm, we have $L_p \leq 10$ μm. Thus, in real structures, where the drift region is about hundreds of micrometers, the relation $L_p << d_0$ is always fulfilled. Therefore, holes take no part in the formation of detector signals. The estimations performed using Eq. (8) show that the hole lifetime is $\approx 10^{-10}$ s. This value coincides to an accuracy of one order of magnitude with the time of hole capture by the deep negatively charged chromium centers (N_{Cr}^-): $\tau_p \equiv \tau_p^- = (\sigma_p^- \cdot \upsilon_p \cdot N_{\mathrm{Cr}}^-)^{-1}$. This value is much lower than the hole transit time between the detector electrodes $t_{\mathrm{tr}} = d_0 / \upsilon_m \cong 5$ ns. At the same time, the electron drift length can be fairly significant. It follows from analysis of the field dependence of electron drift length that in the electric fields $\langle\xi_{av}\rangle \geq 3$ kV/cm, we have $L_n \geq 1$ mm. This means that nonequilibrium electrons will be effectively collected from the track ≥ 1 mm in length. The estimations made using Eq. (8) show that the electron lifetime $\tau_n \geq 10^{-8}$ s, which is comparable with the time of electron capture by the deep neutral chromium centers (N_{Cr}^0): $\tau_n \equiv \tau_n^0 = (\sigma_n^0 \cdot \upsilon_n \cdot N_{\mathrm{Cr}}^0)^{-1}$ and is much higher than the electron transit time between the detector electrodes. Thus, we can conclude that in contrast to ingot semiinsulating LEC SI-GaAs, where the holes are collected [53–58], in the structures compensated by chromium, the current pulse amplitude is mainly determined by collection of electrons from the tracks.

Electric-field strength distribution in the thickness of the sensitive layer is (in accordance with Eq. (4)) a most important characteristic. Simulation and calculation of the equation of electrical neutrality predict that the Fermi level tends to a limit position F_{lim} with increase in compensation degree in detector structures. [59]. In so doing, the specific resistance increases up to the highest value [60]

$$\rho_{\max} = 1/2e \cdot n_i \cdot \sqrt{\mu_n \cdot \mu_p} . \tag{9}$$

Since the Fermi level is pinned on the GaAs surface in the position F_{lim} [59], no free charge depletion region should be formed under formation of metal contacts to the semiinsulating GaAs layer with the highest specific resistance. In this

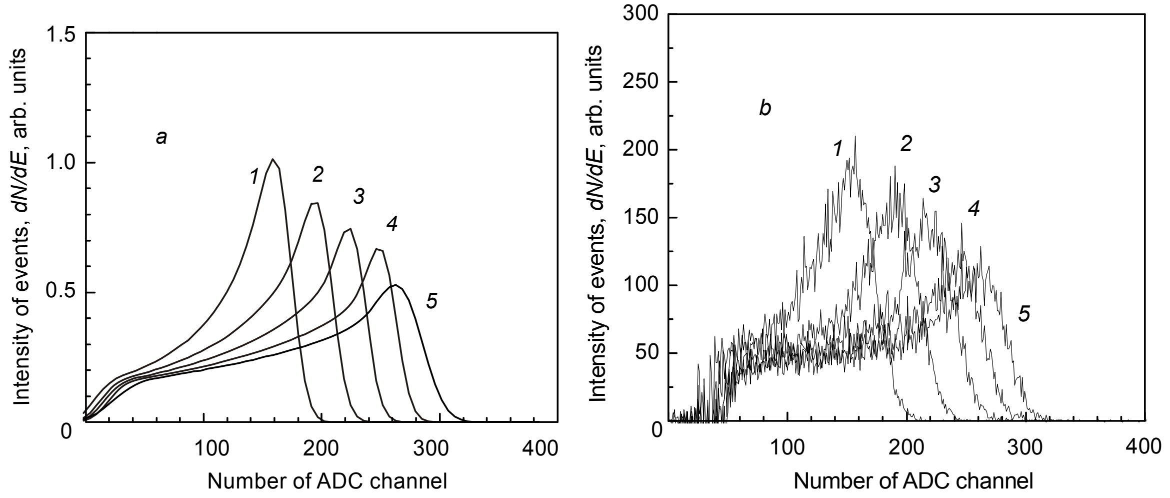

Fig. 1. Calculated (*a*) and experimental (*b*) amplitude spectra of quantum-sensitive detectors based on SI-GaAs(Cr)-structures at various bias voltages applied to the detector, V: 300 (*1*), 400 (*2*), 500 (*3*), 600 (*4*), and 700 (*5*).

case, the distribution of bias voltage applied to the external electrodes of a detector structure should be similar to that of specific resistance of the structure: $\xi(x) \Leftrightarrow \rho(x)$. In fact, in scanning the cleavage of the structure by an optical-point probe, barrier layers are observed to form, however, the volt-ampere characteristic is unaffected. Let us consider, for the sake of simplicity, that we deal with the structures for which the condition $\xi(x) \cong \mathrm{const}(x) =< \xi_{av} >$ is fulfilled.

Formation of current pulses in quantum-sensitive detectors was studied experimentally and compared with the calculation data for the case of gamma-radiation from the ^{241}Am source with the quantum energy 60 keV. A low-energy component of gamma-radiation with the energy 14 keV was cut off by a 300 μm thick GaAs filter. The dependences of the amplitude spectrum and CCE on the bias voltage were studied for the case of single γ-quantum absorption by the sensitive detector layer. Simulation was performed on the basis of the following relation for the energy distribution of event intensity (dN/dE) [61]:

$$\frac{dN}{dE} = \int_0^d \frac{\alpha \cdot \exp^{-\alpha \cdot x}}{\sqrt{2 \cdot \pi} \cdot \sigma_\Sigma(x)\left(1 - \exp^{-\alpha \cdot d}\right)} \cdot \exp\left(\frac{-\left(E - E_{\gamma 0} \cdot \eta(x)\right)^2}{2 \cdot \sigma^2_\Sigma(x)}\right) dx\,, \tag{10}$$

where $\alpha \approx 10.983$ is the absorption coefficient of x-ray radiation with the energy $E_{\gamma 0}$ = 60 keV in GaAs. The Heht function $\eta(x)$ has the form of Eq. (4) in the case of planar detector geometry, the absence of secondary charge-carrier emission, linear dimension of the γ-track much shorter than d_0, and with no allowance for an initial loss. The mean-square deviation of the amplitude of collected charge has the form $\sigma^2_\Sigma(x) = \sigma^2_{st} + \sigma^2_{el} + \sigma^2_{col}(x)$ in the case of independence of noise components, where σ_{st} is the statistic fluctuation of electron-hole pair formation, σ_{el} are the fluctuations caused by noises of electronic equipment, and $\sigma_{col}(x)$ are the fluctuations caused by partial charge collection depending on the point of generation. The amplitude spectra calculated using Eq. (10) for the monoenergy line $E_{\gamma 0}$ = 60 keV of the ^{241}Am isotope at different bias voltages applied to the detector (Fig. 1*a*) coincide with the experimental ones (Fig. 1*b*). No clearly defined monoenergy line is observed in the amplitude spectrum. However, there is a sufficiently extended section in the region of AD-converter small channels. Analysis of Eqs. (4), (5), and (10) makes it possible to conclude that this shape of amplitude spectrum is due to the nonuniform absorption of gamma-radiation in the sample for $L_p << d_0$. The events corresponding to the γ-quantum absorption near the cathode at the

TABLE 1. Types, Characteristics, and Fields of Application of Detectors Developed on the Basis of SI-GaAs(Cr)-Structures

Detector types	Fields of Application	Sensitive region,[1] μm	Coordinate resolution, μm	Number of elements
Microstripped	High-energy physics	52 · 52 · 0.3	50	1024
Pixel	Dental apparatus	12 · 12 · 0.7	170	4096
Pixel	Mammograph	14 · 14 · 0.6	50	65536
Scanning	Mammographic apparatus	26 · 4 · 0.05	100	256
Scanning	X-ray apparatus	26 · 4 · 0.5	200	128
Scanning	Gamma-ray chamber	26 · 10 · 0.5	400	64
Scanning	Defectoscopy	26 · 10 · 0.5	50	512
Scanning	Monitoring systems	32 · 20 · 1	1000	32
Scanning	Safety systems	32 · 10 · 1	1000	32
Unit	α, β, γ, χ, and *n* dosimeters	10 · 10 · 0.3	–	1

[1]Given are the length, width, and height of sensitive regions of detectors

point with the coordinate $x \to 0$, where γ-radiation has the highest intensity, will determine the maximum of amplitude spectrum.

The electron drift length increases with the bias voltage, resulting in the shift of the amplitude spectrum maximum to $E_{\gamma 0}$ and decrease in its absolute value. Note that the area S under the curve of the amplitude spectrum determined as $S = \int_0^\infty \frac{dN}{dE} dE$ is independent of the bias voltage above a certain value of U. This fact along with high CCE allows us to assert that the entire interelectrode space d is an active region (d_0), $d \to d_0$, which is characteristic of resistive structures.

DETECTORS BASED ON COMPENSATED GaAs

The GaAs structures we developed were used for producing quantum-sensitive microstripped and pixel detectors. All the multi-element detectors fabricated using the integrated circuit technology are in essence a big integrated circuit, where the unit elements are the detectors. The simulation and calculation show that if the dimension of the smallest element becomes smaller than the sensitive layer thickness, the charge of the nonequilibrium carrier packet in the point track induces a current pulse while drifting to the anode. The pulse amplitude varies proportionally to $\sim r^{-2}$, where r is the distance between the moving packet and the anode. On recording the minimum ionizing particles, the experimental dependence CCE(U) with attainment of saturation at $\xi \geq 1$ kV/cm is observed to be nonlinear. The maximum value of CCE depends on the thickness of a high-resistance layer and decreases from $\eta \approx 100\%$ at $d_0 \approx 0.4$ mm down to $\eta \approx 65\%$ at $d_0 \approx 1.5$ mm. Analysis of the time characteristics of induced-current pulses shows that practically 100% of electrons are collected from the track, while the holes are partially captured by deep negatively charged Cr centers.

More than 10 different types of detectors have been designed. Their characteristics are given in Table 1.

The configuration of the detector structure presented in Table 1 was chosen on the basis of optimal recording efficiency. For example, for scanning detectors of a given aperture S_a of a unit detector element and scanning time t_c of a unit line, the effective radiation absorption depth d_n is

$$\alpha(E) \cdot d_n \geq \ln\left(\frac{I_0 \cdot S_a \cdot t_c}{I_0 \cdot S_a \cdot t_c - N_0}\right) \cong 0.9 .$$

The topology of certain microstripped, pixel, and scanning detectors designed and fabricated using the integral technology on the basis of SI-GaAs(Cr)-structures is shown in Fig. 2.

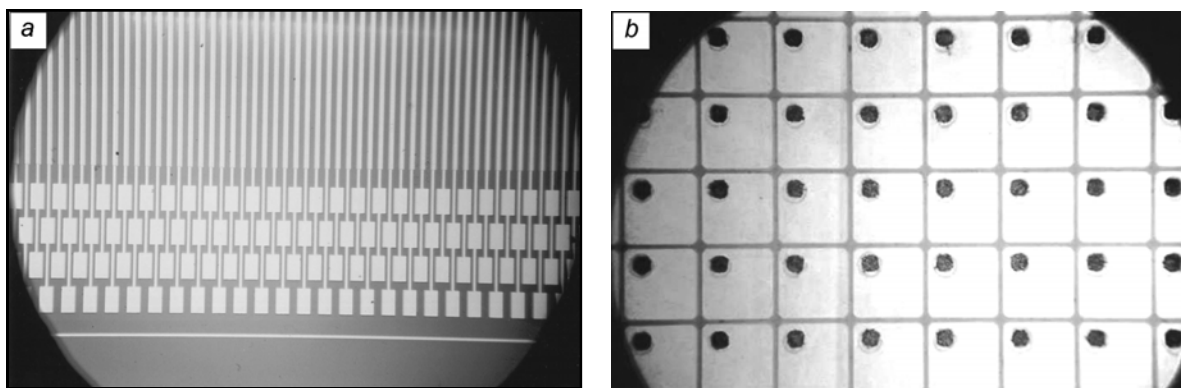

Fig. 2. Fragments of detector chips observed with a microscope at 50-fold magnification: *a* – microstripped detector and *b* – pixel detector.

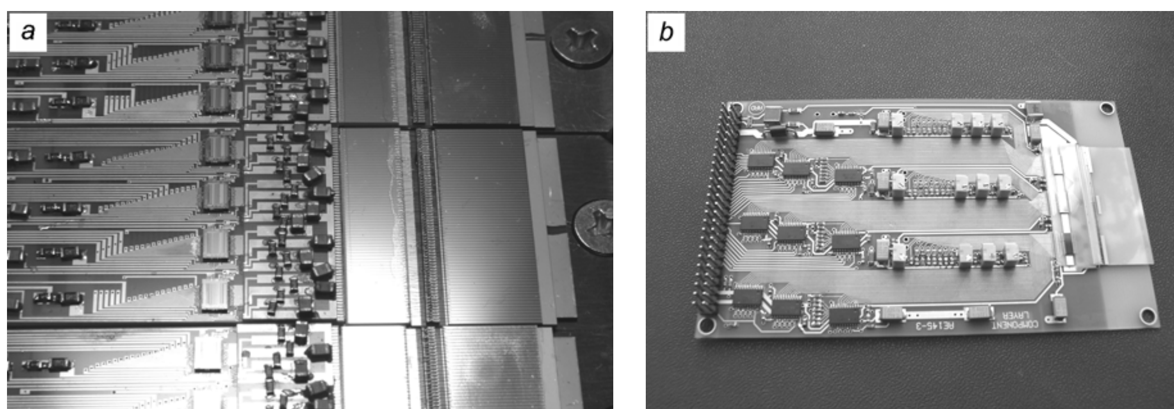

Fig. 3. Digital image modules: for gamma-ray chamber (*a*) and for mammography (*b*).

The microstripped and pixel detectors were used for exact determination of charged-particle coordinates in high-energy physics. For the minimum ionizing particles (MIP), a coordinate resolution of 14 μm was reached. All three detector types are also widely used for constructing modules of the x-ray and gamma-ray digital images. The term "digital" means that the detectors provide counting of single quanta with the energies higher than 10 keV. Further, without special detail, we illustrate some original engineering products on the basis of quantum-sensitive detectors.

MODULES AND SYSTEMS OF DIGITAL X-RAY IMAGES

X-ray and gamma-ray digital image modules with the spatial resolution up to 5,6 line pairs per millimeter, dynamic range 10^3, threshold contrast to 0.5%, and the radiation influence on the object tens times less than that of conventional analogs are designed on the basis of quantum-sensitive detectors. Each of the single quanta of x-ray or gamma radiation is transformed into the current pulse in each individual channel of the scanning strip. The pulses are then amplified and converted into the format "understandable" to the ADC. As a result, the spatial distribution of intensity is converted into a digital code channel by channel.

The digital image modules are shown in Fig. 3.

Figure 4 shows photos of different scanning systems. The individual image modules are connected in a unified multichannel system with vertical line scanning.

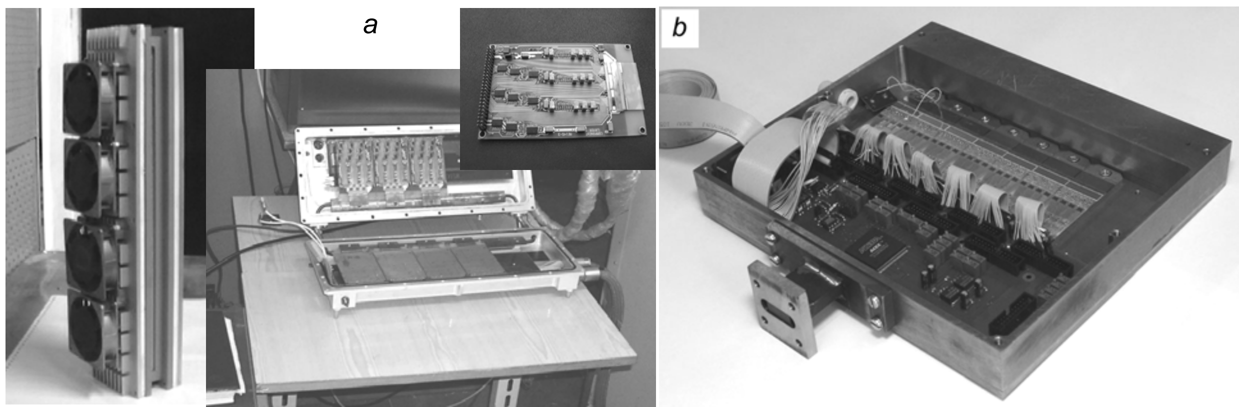

Fig. 4. Scanning digital systems: scanning 4096-channel x-ray systems (*a*) and scanning 1024-channel digital gamma-ray chamber (*b*).

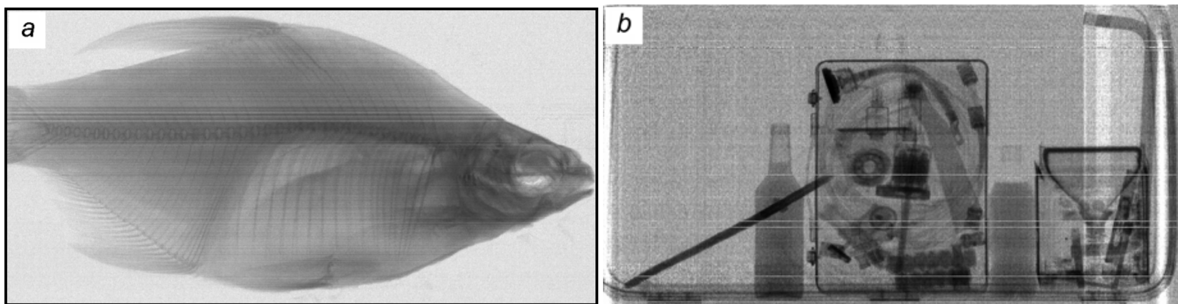

Fig. 5. Images of some low-contrast objects obtained using the detector systems shown in Fig. 4: a fish (*a*) and a bag filled with different things (*b*). $E_\gamma = 3$ MeV.

Figure 5 demonstrates the images of some low-contrast objects obtained using the detector systems shown in Fig. 4.

A full frame of a dried fish from head to tail was formed for 2 s. A single line was scanned for 5 μs. Analysis of the image quality and fine structure of fish anatomy indicates that the threshold contrast better than 0.5% is attained in the experiment.

A STUDY OF RADIATION RESISTANCE OF GaAs DETECTORS

As pointed out above, the next generation of synchrotron sources will produce high-intensity gamma-quantum beams. This demands radiation-resistant gamma-detectors to be designed. Within the framework of the ILC (*International Large Collider*) project, joint research on designing radiation-resistance detectors was performed in 2007 by the Joint Institute of Nuclear Research, Dubna and V. D. Kuznetsov Siberian Physical–Technical Institute at Tomsk State University, Tomsk. The radiation resistance of compensated-GaAs sensors was measured. The samples prepared in Tomsk represent a variant of detectors for an electromagnetic calorimeter FCAL [62]. A general view of the detector is shown in Fig. 6. The size of one detector is ~5×5 mm.

The detectors were tested using an SDALINAC accelerator in Darmstadt, Germany. The arrangement of experimental structures on the accelerator-beam propagation path is shown in Fig. 7. The lateral beam dimension is formed by a 1 cm thick copper collimator. The beam incident onto a detector located in a light intercepting box, is directed into the Faraday cup, and the beam current is measured.

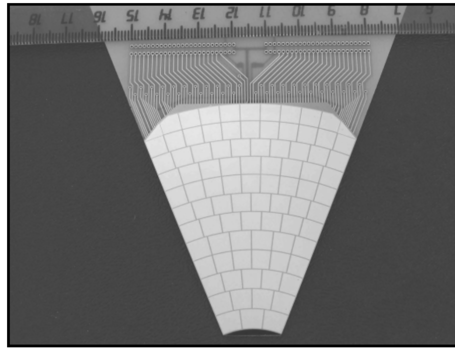

Fig. 6. A general view of the detector for a FCAL-calorimeter prototype.

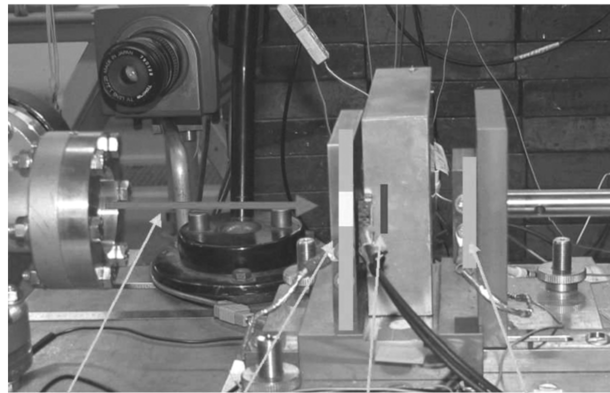

Beam Collimator Detector Faraday cup

Fig. 7. An experimental facility for detector irradiation.

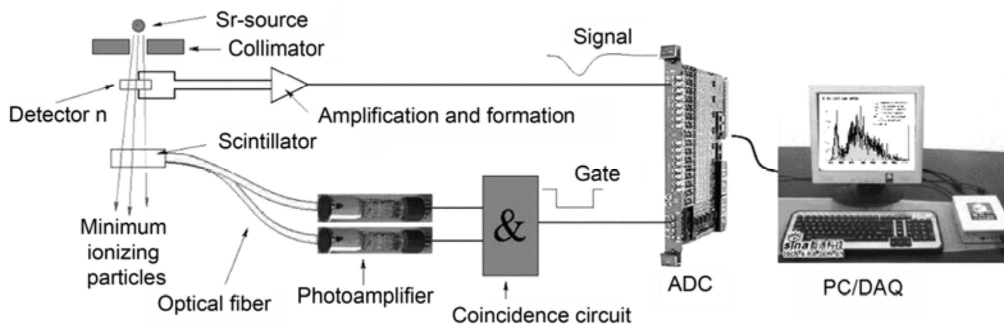

Fig. 8. A system flowchart for measuring sample responses to charged particles.

The effect of detector irradiation by a 10 MeV electron beam was observed using repeatable measurements of the calibration spectra from a radioactive Sr^{90} source (Fig. 8). The electrons from the radioactive source penetrated through the sample and were recorded in a scintillator. The coincidence of signals from two photomultipliers formed a trigger pulse for the ADC and computer recording of the detector signal. The results obtained are shown in Fig. 9.

It is seen from these data that despite the fact that the amplitude of the detector signal decreases under irradiation by 10 MeV electrons (right peak), the detector dark current is practically unaffected (left peak), which

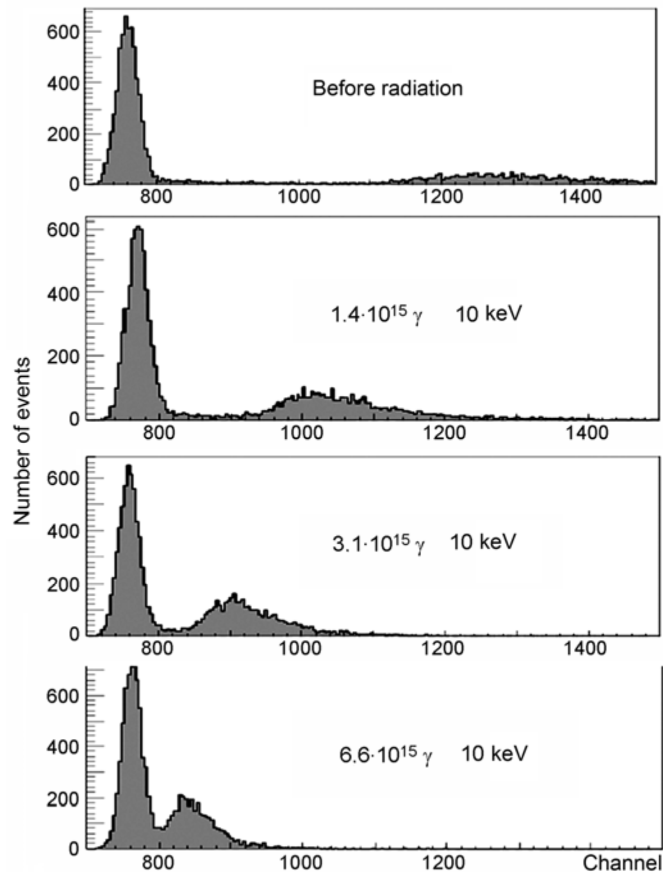

Fig. 9. Variations in the amplitude of GaAs-detector signal versus radiation dose under irradiation by a 10 MeV electron beam (given are the equivalent doses).

provides reliable signal detection up to the dose equivalent to irradiation by a gamma-quantum flux of $\sim 6 \cdot 10^{15}$ γ/cm^2 with $E_\gamma = 10$ keV.

CONCLUSION

In recent ten years, radical changes concerning generation of high-intensity x-ray gamma-radiation beams have occurred. A technique for using synchrotron radiation for static studies and measurement of objects in the nanometer range with femtosecond resolution has been developed and widely applied. This technique is being further extensively developed and the sources of monochromatic coherent x-ray radiation of femtosecond duration are constructed on the basis of X-ray Free Electron Lasers. The methods developed in the course of designing gamma-ray detectors for the purposes of fundamental studies in microworld physics and practical applications in nanotechnologies make it possible to design advanced semiconductor detectors effectively recording nanometer object images. One of the most promising detector materials is GaAs extensively studied by Russian scientists. All of the above provides reason enough to expect the derivation of new scientific and practical solutions to current technical problems in the coming years.

REFERENCES

1. N. Meshkov, E. L. Saldin, E. A. Schneidmiller, *et al*., Perspective of DESY for the fourth generation SR facility, EPAC, 660–663 (2000).
2. Y. Holler, A. Chesnov, E. Matyushevsky, *et al*., Magnetic measurements of the FLASH infrared undulator, FEL 07, Novosibirsk, 2007.
3. J. Bittner, J. Feldhaus, U. Hah, *et al.*, MCP-based photon detector with extended wavelength range for FLASH FEL 07, Novosibirsk, 2007.
4. R. Abeda, M. Altarelli, R. Brinkmann, *et al*., XFEL The European X-ray Free Electron Laser. Technical design report, DESY, 097, 2006.
5. Physical Encyclopaedia, (A. M. Prokhorov, ed.), Great Russian Encyclopaedia, Moscow, 1995.
6. ATLAS Inner Detector Technical Design Report, CERN/LHCC/97-16, ATLAS TDR 4, 30, 1997.
7. Radiation Imaging Detectors, (K. M. Smith and J. Visschers, eds.), Proc. 3rd Intern. Workshop, Amsterdam, The Netherlands, 2002.
8. V. B. Chmill, A. V. Chuntonov, S. S. Khludkov, *et al*., Nucl. Instrum. Methods Phys. Res., **A395**, 65–70 (1997).
9. S. S. Khludkov, L. S. Okaevitch, A. I. Potapov, and O. P. Tolbanov, *Ibid*., **A395**, 132–133 (1997).
10. S. S. Khludkov, O. B. Koretskaya, L. S. Okaevitch, *et al*., *Ibid*., **A410,** 36–40 (1998).
11. V. B. Chmill, A. V. Chuntonov, Falaleev, *et al*., Nucl. Instrum. Methods Phys. Res., **A410,** 54–60 (1998).
12. V. B. Chmill, A. V. Chuntonov, S. S. Khludkov, *et al*., Nucl. Instrum. Methods Phys. Res., **A415,** 247–250 (1998).
13. G. I. Ayzeshtat, A. P. Vorob'ev, O. B. Koretskaya, *et al*., Elektron. promyshl., No. 1–2, 102–106 (1998).
14. D. L. Budnitskii, O. P. Tolbanov, and S. S. Khludkov, Russ. Phys. J., No. 8, 768–772 (1998).
15. O. P. Tolbanov, GaAs structures compensated with deep centers, WIRESCRIPT Journal, CYEN Technologies SRL (1999).
16. V. B. Chmill, A. V. Chuntonov, A. G. Kholodenko, *et al.*, Nucl. Instr. Methods Phys. Res., **A438**, 362–367 (1999).
17. G. I. Ayzeshtat, V. G. Kanaev, A. V. Khan, *et al*., *Ibid*., **A448**, 188–189 (2000).
18. G. I. Ayzeshtat, O. P. Tolbanov, and A. P. Vorob'ev, *Ibid*., **A466**, 1–8 (2001).
19. G. I. Ayzeshtat, N. N. Bakin, D. L. Budnitskii, *et al.,* Nucl. Instrum. Methods Phys. Res., **A466**, 25–32 (2001).
20. D. L. Budnitskii, V. P. Germogenov, *et al.,* Nucl. Instrum. Methods Phys. Res., **A466**, 33–38 (2001).
21. G. I. Ayzeshtat, V. G. Kanaev, A. V. Khan, *et al*., *Ibid*., **A466**, 162–167 (2001).
22. G. I. Ayzeshtat, D. L. Budnitskii, O. B. Koretskaya, *et al*., *Ibid*., **A466**, 96–101 (2001).
23. G. I. Ayzeshtat, D. L. Budnitskii, O. B. Koretskaya, *et al*., *Ibid*., **A494**, 120–127 (2002).
24. G. I. Ayzeshtat, O. P. Tolbanov, and A. P. Vorob'ev, *Ibid*., **A494**, 199–204 (2002).
25. G. I. Ayzeshtat, M. V. Bimatov, O. P. Tolbanov, and A. P. Vorob'ev, *Ibid*., **A494**, 210–213 (2002).
26. S. N. Golovnia, S. A. Gorokhov, O. B. Koretskaya, *et al., Ibid*., **A494**, 223–228 (2002).
27. G. I. Ayzeshtat, D. Yu. Mokeev, O. P. Tolbanov, and A. V. Khan, *Ibid*., **A494**, 229–232 (2002).
28. G. I. Ayzeshtat, A. P. Vorob'ev, V. I. Kudravtsev, and O. P. Tolbanov, Elektron. promyshl., No. 1–2, 20–25 (2002).
29. G. I. Ayzeshtat, M. V. Bimatov, A. P. Vorob'ev, and O. P. Tolbanov, *Ibid*., No. 1–2, 26–28 (2002).
30. V. N. Brudnyi, A. I. Potapov, and O. P. Tolbanov, *Ibid*., No. 1–2, 29–31 (2002).
31. G. I. Ayzeshtat, E. N. Ardashev, A. P. Vorob'ev, *et al., Ibid*., No. 1–2, 32–36 (2002).
32. O. B. Koretskaya, V. A. Novikov, L. S. Okaevitch, *et al*., *Ibid*., No. 1–2, 37–39 (2002).
33. G. I. Ayzeshtat, M. D. Vilisova, A. P. Vorob'ev, *et al*., *Ibid*., No. 1–2, 40–45 (2002).
34. Yu. Baiko, A. P. Vorob'ev, V. P. Germogenov, *et al*., *Ibid*., No. 1–2, 46–53 (2002).
35. M. D. Vilisova, E. P. Drugova, I. Yu. Poltavets, *et al*., *Ibid*., No. 1–2, 53–55 (2002).
36. P. Vorob'ev, O. B. Koretskaya, L. S. Okaevitch, *et al*., *Ibid*., No. 1–2, 56–60 (2002).
37. P. Vorob'ev, O. B. Koretskaya, L. S. Okaevitch, *et al*., *Ibid*., No. 1–2, 60–65 (2002).
38. G. I. Ayzeshtat, D. Yu. Mokeev, O. P. Tolbanov, and A. V. Khan, *Ibid*., No. 1–2, 66–68 (2002).

39. G. I. Ayzeshtat, M. V. Ardyshev, N. G. Kolin, *et al*., *Ibid*., No. 1–2, 69–72 (2002).
40. D. L. Budnitskii, O. B. Koretskaya, V. A. Novikov, *et al*., *Ibid*., No. 1–2, 108–114 (2002).
41. G. I. Ayzeshtat, E. A. Babichev, S. E. Baru, *et al*., Nucl. Instrum. Methods Phys. Res., **A509**, 34–40 (2003).
42. S. N. Golovnia, S. A. Gorokhov, O. B. Koretskaya, *et al.*, *Ibid*., 40–47 (2003).
43. D. L. Budnitskii, O. B. Koretskaya, L. S. Okaevich, *et al*., Nucl. Instrum. Methods Phys. Res., 268–274 (2003).
44. G. I. Ayzeshtat, M. V. Bimatov, O. P. Tolbanov, and A. P. Vorobiev, *Ibid*., **A509**, 52–56 (2003).
45. G. I. Ayzeshtat, V. P. Germogenov, S. M. Guschin, *et al.*, Nucl. Instrum. Methods Phys. Res., **A531**, 97–102 (2004).
46. J. E. Carroll, Hot Electron Microwave Generators, Cambridge University, 1970.
47. R. Trammell and F. J. Walter, Nucl. Instrum. Methods., **A76**, 317–321 (1969).
48. GaAs Detectors and Related Compounds (S. D'Auria and K. M. Smith, eds.), Proc. IV Workshop, Aberfoyle, Scotland, 1996.
49. V. Markov, *et al*., Nucl. Instrum. Methods Phys. Res., **A466**, 14–24 (2001).
50. M. Rogalla and K. Runge, *Ibid*., **A434**, 44–56 (1999).
51. M. Rogalla, *et al*., *Ibid*., **A410**, 74–78 (1998).
52. GaAs Detectors and Related Compounds (K. M. Smith and S. D'Auria, eds.), Proc. V Workshop, Udine, Italy, 1997.
53. Quaranta, C. Canali, A. Cavallini, *et al*., Nucl. Instrum. Methods Phys. Res., **A380**, 201–204 (1996).
54. GaAs Detectors and Related Compounds (S. Pospisil and K. M. Smith, eds.), Proc. VI Workshop, Praha-Pruhonice, Czech Republic, 1998.
55. Radiation Imaging Detectors (C. Frojdh and S. Petersson, eds.), Proc. 1st Workshop. Sundsvall, Sweden, 1999.
56. Radiation Imaging Detectors (J. Ludwig and L. Feld, eds.), Proc. 2nd Workshop. Freiburg, Germany, 2000.
57. K. M. Smith, *et al.*, Nucl. Instrum. Methods Phys. Res., **A460**, 204–206 (2001).
58. Science, Technologies, Products, Anniversary Edition of Federal State Enterprise - Research Institute of Semiconductor Devices, Electronnaya promyshl., No. 2–3, 210 (2002).
59. V. N. Brudnyi, Author's Abstract of Doct. Chem. Sci. Thesis, Tomsk, 1993.
60. K. Seeger, Semiconductor Physics, Springer Verlag, Wein, New York, 1973.
61. E. M. Verbitskaya, *et al.*, Fiz. Tekh. Poluprovodn., **27**, No. 12, 2052–2067 (1999).
62. G. Grah, R. Heller, H. Henschel, *et al*., Radiation hard sensors for the beam calorimeter of the ILC in: Proc. the IEEE Nuclear Science Symposium (NSS) and Medical Imaging Conference (MIC), Honolulu, Hawaii, 2008.